14 A Mesoscopic–Microscopic Perspective on Ion Channel Permeation Energetics: The Semi-Microscopic Approach[1]

Peter C. Jordan

14.1 Introduction

Understanding how physiological ion channels simultaneously exhibit the apparently contradictory properties of high throughput and great discrimination is a long-standing theoretical problem. These nanodevices all operate on the same basic principle: ions, solvated by bulk water, lose a significant part of their hydration shell as they pass through a constriction where a chemical selection process occurs (Hille, 2001). High throughput requires that the chosen ion faces no significant energy barrier, which would forbid its entry. On first blush, it seems that falling into a deep well is also forbidden, since that would apparently trap it in the channel and block further passage. While generally true, some channels function in multi-ion mode, so that they are permanently ion-occupied; permeation then occurs with the entry of a second (or third) ion, repelling the prior occupant and leading to conduction. In all instances, high selectivity requires that there is a mechanism by which all other physiologically prevalent ions face significant energetic discrimination.

The theoretical tools for studying permeation are of two basic types. Continuum approaches describe ions by Poisson–Boltzmann theory, as charge distributions with associated ion atmospheres, in essence extending the standard description of electrodiffusion to account for the influence of bulk electrolyte. This Poisson–Nernst–Planck (PNP) theory is computationally efficient (Chen et al., 1992; Eisenberg, 1999). It directly assesses how changes in a protein's ~~charge~~ electrical structure and physical geometry affect channel conductance. However, it is parameter rich, requiring input assumptions regarding channel geometry, ionic diffusion coefficients and the local channel dielectric constant, $\varepsilon(\mathbf{r})$, all of which hard to substantiate. A local ε is an exceptionally nebulous concept; it cannot be rigorous, since the dielectric constant is a generalized susceptibility (Partenskii and Jordan, 1992). In nonuniform surroundings, it is not surprising that different measures of electrical response lead to different ε estimates (Jordan et al., 1997). The PNP approach is a reliable tool for wider channels (Im and Roux, 2002). For narrow, selective channels, in addition to

[1] Portions reprinted, with permission, from P.C. Jordan, "Semimicroscopic Modeling of Permeation Energetics in Ion Channels," *IEEE Transactions on Nanobioscience*, 4:94–101 [2005], IEEE.

properly choosing ε, there is another serious concern. A permeant ion cannot carry an ion atmosphere with it into the interior of a narrow channel (Corry et al., 2000; Moy et al., 2000).

Brownian dynamics (BD) is an alternate way to directly compute I–V profiles (Chung et al., 2002a). Here ions are discrete, and a channel's charge distribution effectively forbids counterion entry into selective confines. Ions move in a field determined by protein charges and are impeded by viscous drag due to the surrounding (continuum) water. The influence of bulk electrolyte is relatively easily taken into account. As with PNP, BD requires assumptions with respect to a channel's physical and dielectric geometry. Carefully parameterized it is a valuable correlational tool for analyzing electrical behavior in narrow channels (Chung et al., 1999, 2002b; Corry et al., 2004).

Given the enormous advances in computational power, and the undoubted success of computational chemistry in the analysis of the properties of (water soluble) proteins, molecular dynamics (MD) would appear ideal for relating structure and function. However, realizing this goal has been difficult, in part reflecting technical problems, in part for more fundamental reasons. Even with massively parallel computing, direct monitoring of ion transit through a highly selective channel is not yet possible. To simulate an ion channel embedded in a phospholipid membrane and sandwiched between electrolyte layers typically involves some 10^5 atoms; heroic computations follow dynamics for $\leq$100 ns, easily an order of magnitude less than the fastest ion transit times. Efforts to circumvent these difficulties in the prototype potassium channel, KcsA, have been made using a microscopic–mesoscopic approach (Burykin et al., 2002). Current has however been directly simulated in the large bore system, α-hemolysin, where simulations of 1 ns duration are adequate for reliable statistics (Aksimentiev and Schulten, 2005). Most often, rather than attempting to directly observe ion translocation, MD is used to compute the free energy for transferring an ion from electrolyte into the channel, the so-called potential of mean force (PMF) (Bernèche and Roux, 2003). Combined with an ionic diffusion coefficient (also obtained from MD) a PMF can then indirectly determine the ion channel conductance (Allen et al., 2004) .

However, this protocol is only as reliable as the underlying PMF. Gramicidin, a structurally superbly well-characterized, extremely narrow ion channel (Ketchem et al., 1997), is a case where MD misleads. In this system, which accommodates ∼9 water molecules in a linear array, either of two conventional force fields yields a translocational free energy barrier for potassium passage of ∼50 kJ mol^{-1} at 300 K; in 0.1 M electrolyte this implies a single-channel conductance of $\sim 10^{-7}$ pS, about seven orders of magnitude less than that observed (Allen et al., 2003). What may have gone wrong? Simulations are never totally faithful representations of macroscopic reality. Only a thin layer of electrolyte is simulated, but a technical trick, the use of periodic boundary conditions, to a large extent compensates for this limitation. More problematical are the force fields themselves. They are classical substitutes for quantum mechanics. Atoms are assigned fixed effective partial charges, determined by a variety of parameterization methods. But during permeation ions pass close

Au: Is this running head okey?

to channel moieties, polarizing charge distributions. Water models most clearly illustrate the possible difficulties in ion channel simulation. They are designed to reproduce behavior of bulk liquid water, where four or five near neighbors typically surround each molecule. Their charge distributions, with dipole moments of ∼2.2–2.4 Debye, reflect mean liquid properties. As water's gas phase dipole moment is 1.85 Debye, water–water interaction has substantially altered the molecules' charge distributions. In a narrow ion channel like gramicidin, where water molecules line up single file, the environment is vastly different from the network structure of bulk water. Here polarization may be expected to have affected water's charge distribution differently, with uncertain consequences. In other words, the more the simulational surroundings differ from ambient water, the less reliable a conventional, nonpolarizable water model is likely to be.

The semi-microscopic (SMC) approach is designed to circumvent many of these problems (Dorman et al., 1996; Dorman and Jordan, 2003, 2004; Garofoli and Jordan, 2003). It is a conceptually transparent simplification of biophysical reality, one that is readily extendable. It exploits the time scale separation between electronic and structural contributions to dielectric stabilization, dealing with electronic polarization by embedding the channel in surroundings that account for polarization in a mean sense. The reorganizational contribution to dielectric stabilization is ascribed to a limited set of mobile entities: ions, water, and selected peptide moieties. This approach forms a bridge between continuum electrostatic modeling and MD, avoiding two of MD's major limitations: force fields that don't account for electronic polarization; potential electrostatic artifacts introduced by periodic boundary conditions. It permits ready deconvolution of individual moieties' influence on permeation free energies and relatively easily contrasts the behavior of different permeant species, thus directly addressing selectivity. Advantages and limitations of the technique are described. Methodological details are outlined and applied to three convenient dielectric geometries. Practical aspects of the SMC procedure are explained, highlighting some areas ripe for further development. Finally, some specific applications are considered.

14.2 Electronic Polarization and the Dielectric Background

The physical observation central to the SMC method is that dielectric reorganization, which is responsible for the solvating ability of polar media, cleanly separates into structural and electronic components. This is always true, regardless of whether a system is uniform (like bulk water) or massively nonuniform (like the surroundings of ion channel selectivity filters). Ligand response to permeant species movement is described by structural terms. Electronic terms account for permeation-induced reorganization of the solvent (here water, peptide, and lipid) charge distribution. The two time scales differ vastly. Electrons rearrange in femtoseconds, while structural

relaxation occurs over a wide time span. But even the fastest such contributions, due to translation and vibration, are at least 100 times slower. Water is typical. At low frequencies (<100 GHz) it exhibits bulk dielectric properties. At higher frequencies water rotates or translates too slowly to respond to electrical stress; in effect these degrees of freedom are frozen and ε drops to its optical value, $\sim$1.8 (Hasted, 1973). In an essentially Born–Oppenheimer-like approximation structural change takes place with the electron distribution relaxed. A first approximation treats the electronic background as uniform, with a roughly universal polarizability representative of lipids (Fettiplace et al., 1971) as well as water; in essence molecular realignment occurs under conditions where $\varepsilon \sim 2$.

The SMC treatment exploits this time scale separation, extending semi-microscopic approaches discussed in the study of Helmholtz layers at electrode–electrolyte interfaces, where explicit reorientable electrical sources are placed in interfacial background dielectrics with an assigned ε, $\sim$2–3 (Kornyshev, 1988). Our SMC work accounts for electronic polarization by locating the mobile moieties in a dielectric background with $\varepsilon = 2$. It treats structural influences to dielectric shielding by explicitly including those charged features of the peptide–lipid–water ensemble that interact strongly with the permeant. As these contributions to charge stabilization arise from translation and rotation of charged and polar elements in the surroundings (the generalized solvent), a sufficient number of these must be mobile for this simplification to be effective. Thus, for the SMC approach to be more generally applicable requires extensive parameterizations, similar to those familiar in constructing the force fields of computational chemistry (van Gunsteren and Berendsen, 1987; Cornell et al., 1995; MacKerell et al., 1998).

14.3 Long-Range Electrostatics and Model Geometries

Standard MD simulations impose severe computational loads. In order to model both cytoplasmic and extracellular water, the channel–lipid assembly is surrounded by extended regions of aqueous solvent; simulating these is generally the most costly part of the computation. Due to boundary effects, simulations with as many as $\sim 10^5$ atomic centers may still not be representative of bulk. Periodic boundary conditions are used to reduce the associated errors; however as electrostatic forces are long-range, great care is required to correct for electrical cutoffs in treating the reaction field.

The SMC approach avoids this problem by embedding the membrane–peptide–ion channel ensemble in electrical geometries where generalized image methods rigorously determine the reaction field. This is the crux of the technique, and is described in detail. Figure 14.1 illustrates a specific SMC simplification, one designed to approximate the potassium channel selectivity filter. It is based on the structure of the KcsA potassium channel (Doyle et al., 1998), and generates a tractable computational model. Explicitly modeled features are in the interior, low ε region. The

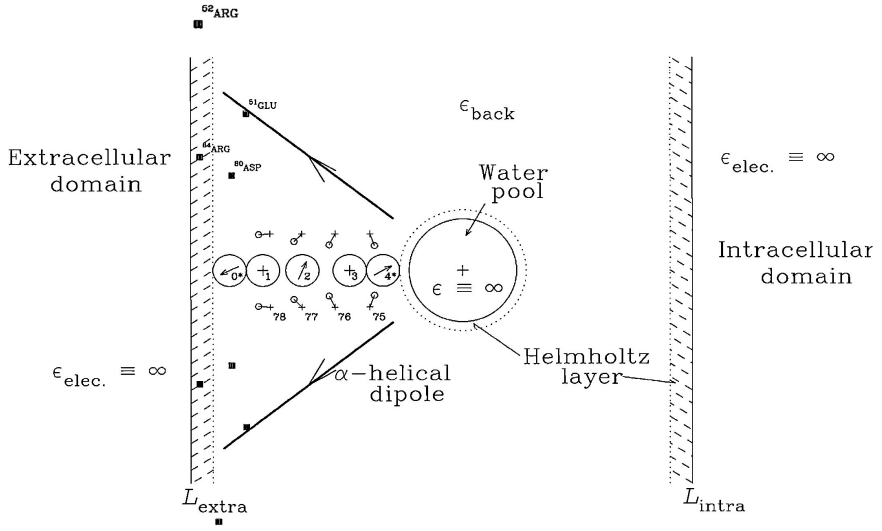

Fig. 14.1 SMC model of an ion, water, KcsA filter, lipid, and electrolyte system (Garofoli and Jordan, 2003). The planar projection shows single file ions and waters, the coordinating carbonyl groups, peptide dipoles, selected charged residues, the aqueous cavity, and an included ion. Ions, waters, and carbonyl oxygens (numbered 75–78) are mobile. Helmholtz layers account for water orientationally immobilized by interaction with polar and/or ordered species at dielectric boundaries; explicit sources are forbidden from penetrating these regions. The pool accommodates ∼20 water molecules. Numbering follows the convention of Morais-Cabral et al. (2001). Reprinted from Garofoli and Jordan (2003) with permission.

water pool approximates a major feature of potassium channels, their mid-membrane water-filled cavities. Sharp electrical boundaries demarcate the different regions.

Three tractable computational geometries are illustrated in Fig. 14.2. As for the case of Fig. 14.1, the low permittivity, ε_1 domain contains all explicitly modeled charges; the ε_2 surroundings dielectrically mimic (or closely approximate) bulk water. Figure 14.2a, with its parallel boundaries, is simplest and exactly treatable. The reaction field for a charge q, located at $\mathbf{R} = z\mathbf{k}$ in a slab of width W, is rigorously described by a set of oscillating image charges, their locations determined by successive reflection at alternating planar boundaries,

$$q_n = (-)^n[(\varepsilon_2 - \varepsilon_1)/(\varepsilon_2 + \varepsilon_1)]q, \quad \mathbf{R}_n^{\pm} = [\pm nW + (-)^n z]\mathbf{k}, n > 0; \quad (14.1)$$

from these, the charge's polarization energy and the reaction field contribution to interaction with other explicit charges is found by summing the coulombic interaction energy of every explicit charge with the whole image set.

Reaction field energetics for the Fig. 14.2b and c geometries only has approximate image equivalents. However, in all applications of interest, the two dielectric domains are vastly dissimilar, $\varepsilon_2 \gg \varepsilon_1$, and simplification, by assuming that $\varepsilon_2 \equiv \infty$, introduces insignificant error (Dorman and Jordan, 2003). In this limit,

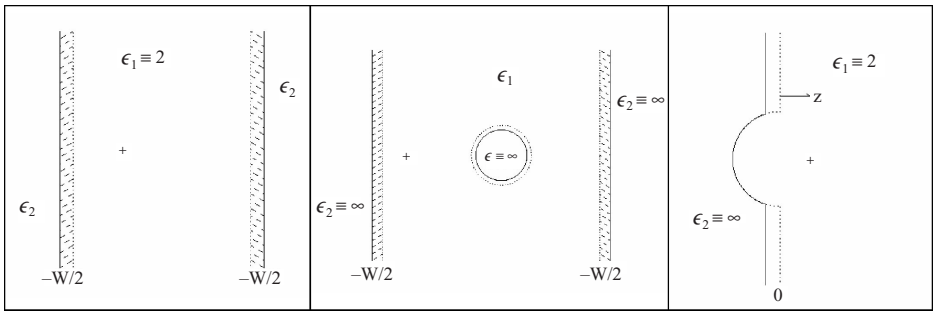

Fig. 14.2 Three electrical geometries used in SMC studies. Explicit electrical sources are in the low permittivity region; for specificity a single positive source is included. All geometries yield analytical expressions for the reaction field. (a) Slab of width W. (b) Slab of width W with a water-like cavity. (c) Semi-infinite bubble geometry. Hatched regions in (a) and (b), and region between solid and dotted lines in (c) are Helmholtz layers (see text and Fig. 14.1 caption). Reprinted from Jordan (2005) with permission.

image methods are again reliable. The geometry of Fig. 14.2b includes the potassium channel's mid-channel water pool (Doyle et al., 1998), illustrated in Fig. 14.1. Instead of explicitly describing the ∼20–25 water molecules that occupy this region, this inner ~~pore~~ is assigned a high permittivity, $\varepsilon \to \infty$. Images for a charge at **R** in the ε_1 region are generated iteratively, and must include the influence of the two bulk electrolyte regions as well as that of the water pool. For the geometry illustrated, a sphere of radius a_o, centered in the middle of a slab of width W, the first images arising from interaction with bulk water are the solutions of Eq. 14.1 for $n = 1$ and $\varepsilon_2 \equiv \infty$. Interaction with the spherical cavity creates an image charge q' at **S**,

$$q' = -q(a_o/R), \qquad \mathbf{S} = (a_o/R)^2\mathbf{R}. \tag{14.2}$$

As image interaction makes the cavity effectively dipolar, not charged, a compensating charge is required at the cavity center.

An explicit charge generates four primary images, one in each bulk region and a dipolar pair in the cavity. Repeating the procedure, each of these generates further images with oscillating polarity. Bulk phase images spawn three new images, one in the other bulk phase and two in the cavity, one of which is at the origin. Each cavity image spawns two new ones, one in each bulk phase. The total number grows very rapidly and doesn't sum to closed form. However, the cavity dipolar images attenuate rapidly; only the first two must be considered. The series of purely planar images oscillates rapidly; beyond tenth order they can be ignored (Garofoli and Jordan, 2003).

The Fig. 14.2c geometry was designed for a much different purpose. SMC model geometries have sharp electrical discontinuities between continuum, bulk-like dielectric regions and the low permittivity, ε_1 domain, which harbors the explicit,

mobile charges. This is problematical for two reasons: charges near a boundary interact directly with molecules in the bulk solvent domain in ways that are sensitive to structural details; in reality electrical boundaries are never sharp. Neither is accounted for by the model geometries of Fig. 14.2a and b. The closer a charge is to a boundary, the more its reaction field is subject to discontinuity-related artifacts and the less faithfully it reflects ensemble averaged details of interaction between a charged or polar moiety and nearby molecular bulk water. Consequently, we introduced Helmholtz layers as buffer domains (Kornyshev, 1988), but these do not fully eliminate errors arising when sources approach an electrical discontinuity.

An obvious approach is to ensure that charged species exiting the pore or near bulk water domains are fully hydrated. This can be done in two ways. Either insert a large explicit water region between the membrane–protein assembly and the dielectric boundary, which increases the computational load substantially (Miloshevsky and Jordan, 2004), or graft a small water-filled bubble, large enough to fully hydrate an ion at or near the pore mouth, onto the channel mouth. This is illustrated in Fig. 14.2c (Dorman and Jordan, 2004). It is particularly simple; an explicit charge has a single electrical image because there is only one electrical dividing surface. However, the geometry is semi-infinite and only useful if, as is often the case, selectivity and permeation are controlled by structures on one side of the assembly. Fig. 14.3 maps it into an equivalent electrical problem, a right-angled wedge, where the high ε domain subtends one-quarter of the space, for which the electrical potential can be computed (Dorman and Jordan, 2004). The SMC approach, by introducing buffer domains and limiting the computational system to those few water molecules and peptide groups explicitly solvating the ion(s), shares similarities with constraint methods introduced by Warshel (Warshel, 1979; King and Warshel, 1989). Our simplifying decomposition, treating a few solvent molecules explicitly and modeling the surroundings as dielectric continua, also strongly resembles an approach developed by Roux (Beglov and Roux, 1994); however, they don't exploit time scale separation, assigning the region containing explicit moieties an ε of 1.

This reaction field problem is difficult and doesn't have a simple solution like Eqs. 14.1 or 14.2. The confocal transformation of Fig. 14.3 turns the hemispherical bubble separating low and high ε regions into a right-angled wedge, which is an exactly soluble electrostatic problem. R_{elec} is the bubble's electrical radius and the transformation is based on the invariant point where the dashed circle is tangent to the bubble. The electrical equivalents of points on or below the dividing surface are found by inversion through a surface defined by the dashed circle of radius $2R_{\text{elec}}$, centered at point I. The upper panel translates a generic point $\mathbf{r} = (x, y, z)$ along x by $-R_{\text{elec}}$; the translated vector, $\mathbf{r}_{\text{T}} = (x + R_{\text{elec}}, y, z)$ is then inverted, a procedure which requires charge and potential rescaling (Dorman and Jordan, 2003; Jackson, 1962). The inverted vector is

$$\mathbf{r}_{\text{I}} = (2R_{\text{elec}})^2 \mathbf{r}_{\text{T}} / |r_{\text{T}}|^2; \tag{14.3}$$

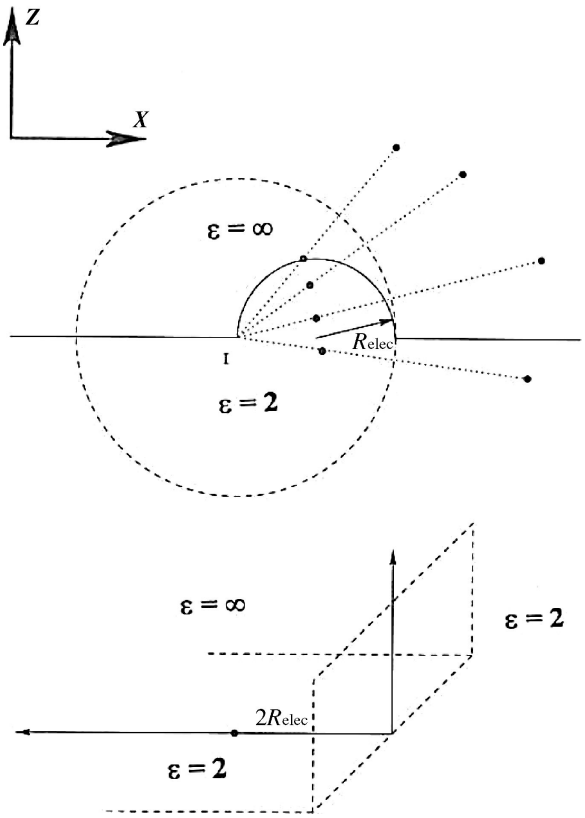

Fig. 14.3 Mapping of bubble geometry of Fig. 14.2c into a wedge. The point I is the inversion center for the transformation. After transformation points on the bubble surface lie on the plane at $x = 2R_{elec}$. The invariant point is where the bubble intersects the inversion sphere. Reprinted from Dorman and Jordan (2004) by permission.

charge and potential rescaling yields

$$q_I = -2R_{elec}q/r_T, \quad \varphi_I = (r_T/2R_{elec})\varphi. \tag{14.4}$$

The x–z projection of the new geometry is illustrated in the lower panel. The hemisphere and the original plane become semi-infinite planes, the new surfaces are ($x_I = 2R_{elec}, -\infty < y_I < +\infty, z_I > 0$) and ($x_I < 2R_{elec}, -\infty < y_I < +\infty, z_I = 0$), respectively. Representative transformed points within the region containing all explicit electrical sources, the hemisphere ($z > 0$) and cylinder ($-R_{elec} < \rho < R_{elec}$, $z < 0$), are shown in the upper panel. Points in the low ε region map into exterior points. Points on the bubble map to points on the surface $x = 2R_{elec}$. In this planar projection the high ε region is the second quadrant. The original bubble geometry is equivalent to a wedge, a solved electrical problem (Smythe, 1968).

Au: Please include this reference in the reference list.

If the angle subtended by the low ε region is $\beta = \pi/p$, the potential at (ρ, α, z) from an electrical source at (ρ_0, α_0, z_0) is

$$\varphi_p = \pi^{-1}[rr_0]^{-1/2} \int_\eta^\infty dx\, f(p, x, \alpha, \alpha_0) K(x, \eta), \tag{14.5}$$

where η, the kernel $K(x, \eta)$ and the function $f(p, x, \alpha, \alpha_0)$ are respectively

$$\cosh \eta = \left[r^2 + r_0^2 + (z - z_0)^2\right]/2rr_0, \tag{14.6}$$

$$K(x, \eta) = (\cosh x - \cosh \eta)^{-1/2}, \tag{14.7}$$

$$f(p, x, \alpha, \alpha_0) = p\, \sinh px [(\cosh px - \cos p(\alpha - \alpha_0))^{-1} - (\cosh px - \cos p(\alpha + \alpha_0))^{-1}]. \tag{14.8}$$

Here, $\beta = 3\pi/2$ and $p = 2/3$. While Eq. 14.5 is well defined, its integrand has singularities requiring careful handling. In determining the source's "self-energy," $[r, z, \alpha] \to [r_0, z_0, \alpha_0]$ where the denominator of the first term in Eq. 14.8 approaches zero. This requires integration over the putative singularity before effecting the limit $[r, z, \alpha] \to [r_0, z_0, \alpha_0]$. The denominator of the second term approaches zero as both $\eta \to 0$ and $\alpha \to \alpha_0 \to 3\pi/2$ and in Eq. 14.7 the kernel, $K(x, \eta)$, is singular as both $\eta \to 0$ and $x \to 0$. These singularities are integrable, and are handled by a reformulation that treats them analytically, all remaining contributions to the reaction field being computed numerically (Dorman and Jordan, 2004). A "dimple" geometry (a wedge angle $\beta = \pi/2$) is much simpler; it can be treated by extensions of standard image approaches since, for all $\beta < \pi$, a point within the low ε region has a unique image. This isn't the case for the "bubble" treated here.

Reflecting the left-hand boundary of Fig. 14.2c, by grafting another bubble onto the right-hand dividing surface of Fig. 14.2a, would generate the "ideal" SMC electrical geometry. Both channel mouths would then be in direct contact with solvent containing bubbles that mimic explicit bulk water. However, this would create two electrical dividing surfaces and each explicit charge, just as in Fig. 14.2a, would generate an infinite set of oscillating images. Unfortunately, this geometry can't be mapped simply; there is no easy way to catalogue images or determine the reaction field potential.

14.4 The Born Energy

SMC modeling of permeation energetics requires transferring ions between dielectrics. A Born charging energy is associated with such processes. Removing an ion (or a polar species) from bulk ambient water and placing it in a dielectric with

$\varepsilon = 2$ is substantially endoergic. For an ion the energy penalty is

$$\Delta G^{\text{ion}}_{\text{aqueous}\rightarrow\varepsilon=2} = -\Delta G_{\text{hydration}} - \frac{1}{2\varepsilon_1 R^{\text{ion}}_{\text{Cav}}}, \tag{14.9a}$$

where the overall free energy change is $\Delta G^{\text{ion}}_{\text{aqueous}\rightarrow\varepsilon=2}$, the ionic hydration free energy is $\Delta G_{\text{hydration}}$ and the radius of the ionic solvation cavity in the ε_1 domain is $R^{\text{ion}}_{\text{Cav}}$. The corresponding expression for water molecule transfer is

$$\Delta G^{\text{water}}_{\varepsilon=2\rightarrow\text{aqueous}} = -\Delta G_{\text{vaporization}} + G^{\text{water}}_{\text{Born}}\left(\varepsilon_1, R^{\text{water}}_{\text{Cav}}\right) \tag{14.9b}$$

(Beveridge and Schnuelle, 1975; Dorman and Jordan, 2003; Dorman and Jordan, 2004); the second term in Eq. 14.9b is analogous to the ionic Born energy of Eq. 14.9a. This transfer of polar moieties between water and a solvation cavity differs fundamentally from that in the Born model of ionic solvation (Born, 1920; Grunwald, 1996). ~~Their~~ solvent is a structureless continuum and its microscopic reorientational influence on dielectric stabilization is incorporated into a Born radius, a parameter in many ways decoupled from the ion's physical size (Papazyan and Warshel, 1998). SMC modeling explicitly treats solvent reorientation, rearranging these surroundings as water is exchanged for an ion. The Born-like term only includes the influence of the dielectric background, i.e., the electronic polarizability. Consequently, and in stark contrast to the Born process that simultaneously accounts for solvent reorganization and electronic polarization, both $R^{\text{ion}}_{\text{Cav}}$ and $R^{\text{water}}_{\text{Cav}}$ can be interpreted simply. They closely approximate an ion's (or a water's) physical radius (Dorman and Jordan, 2003, 2004) and, in general, are only slightly altered by changes in their immediate surroundings, a point to be discussed later.

14.5 Force Field Parameterization

SMC modeling sites explicit electrical sources in an unconventional dielectric background, one with $\varepsilon = 2$. Consequently, standard force fields cannot be used. Ions are described as charged hard spheres, with crystallographic radii (Pauling, 1960). The water charge distribution is a simple point charge (SPC)-like (Berendsen et al., 1981), with charges chosen to reproduce water's permanent dipole moment, a choice required since electronic polarization has been implicitly treated by introducing the background dielectric. The water charges are placed at the atomic centers, embedded in a sphere with the radius of ambient bulk water. This primitive model reproduces the hydration free energies of the smaller halides and all physiologically important alkali cations (Dorman and Jordan, 2003). Carbonyls and amide groups are viewed as rigid dipoles, with standard bond lengths of 1.24 and 0.96 Å, respectively. In all applications to date ions and waters have been in direct contact only with one another and with peptide backbone atoms; the carbonyl oxygens, amide nitrogens, and α-carbons are treated as hard spheres (Dorman and Jordan, 2004). Just as with water,

the other dipolar moieties must be assigned charges representative of their permanent dipoles. Peptide backbones are rigid and CO and NH libration is described by harmonic restoring forces (Garofoli and Jordan, 2003; Dorman and Jordan, 2004).

This procedure has an ad hoc component, and limits the predictive capacity of the SMC approach. Model improvement is possible, but requires a major research investment. To go further entails proceeding as is done in parameterizing more familiar force fields (van Gunsteren and Berendsen, 1987; Cornell et al., 1995; MacKerell et al., 1998). Bonded terms in a force field as well as effective partial charges reflect quantum considerations. These should not change in a dielectric background with $\varepsilon \equiv 2$, rather than vacuum. Instead of assigning hard-core radii, short-range, nonbonded interactions between the various moieties should be described by standard two parameter functions; this could be done by developing a 6–12 (or other) formalism suitable for SMC studies.

14.6 The Thermodynamic Cycle

Permeation is a concerted process. As an ion enters from one side of the channel, another ion or a water molecule departs on the other side. Expressing ion–water exchange in chemical terms yields

$$\mathrm{Ion}_{\mathrm{aqeous}} + \mathrm{Water}_{\mathrm{channel}} \rightarrow \mathrm{Ion}_{\mathrm{channel}} + \mathrm{Water}_{\mathrm{aqeous}}, \tag{14.10}$$

where the subscripts refer to aqueous and channel solvation environments. A channel water molecule gradually mutates into an ion; simultaneously a hydrated ion turns into a water molecule. Each polar moiety is surrounded by a solvation cavity, with which is associated a Born energy. The overall free energy change can be decomposed into an equivalent multistep thermodynamic cycle. Two somewhat different procedures have been devised, depending on the electrical geometry used.

For the KcsA water pool geometry (Figs. 14.1 and 14.2b), there are three intermediate stages in the mutation, illustrated in Fig. 14.4. An ion in bulk is exchanged for water in vacuum, then the gas phase ion is exchanged for a water in the ε_1 dielectric background and finally the ion in this background is exchanged for a water in the channel (Garofoli and Jordan, 2003). This can be expressed as sequential reactions:

$$\mathrm{Ion}_{\mathrm{aqeous}} + \mathrm{Water}_{\mathrm{vacuum}} \rightarrow \mathrm{Ion}_{\mathrm{vacuum}} + \mathrm{Water}_{\mathrm{aqeous}}, \tag{14.11a}$$

$$\mathrm{Ion}_{\mathrm{vacuum}} + \mathrm{Water}_{\mathrm{background}} \rightarrow \mathrm{Ion}_{\mathrm{background}} + \mathrm{Water}_{\mathrm{vacuum}}, \tag{14.11b}$$

$$\mathrm{Ion}_{\mathrm{background}} + \mathrm{Water}_{\mathrm{channel}} \rightarrow \mathrm{Ion}_{\mathrm{channel}} + \mathrm{Water}_{\mathrm{background}}, \tag{14.11c}$$

and the new subscripts refer to intermediate residence in the dielectric background and vacuum. In the first two steps the permittivity of the solvent changes; the total free energy change is given by summing Eq. 14.9a and Eq. 14.9b. The last step, which involves interaction with the channel peptide, takes place in the uniform, ε_1,

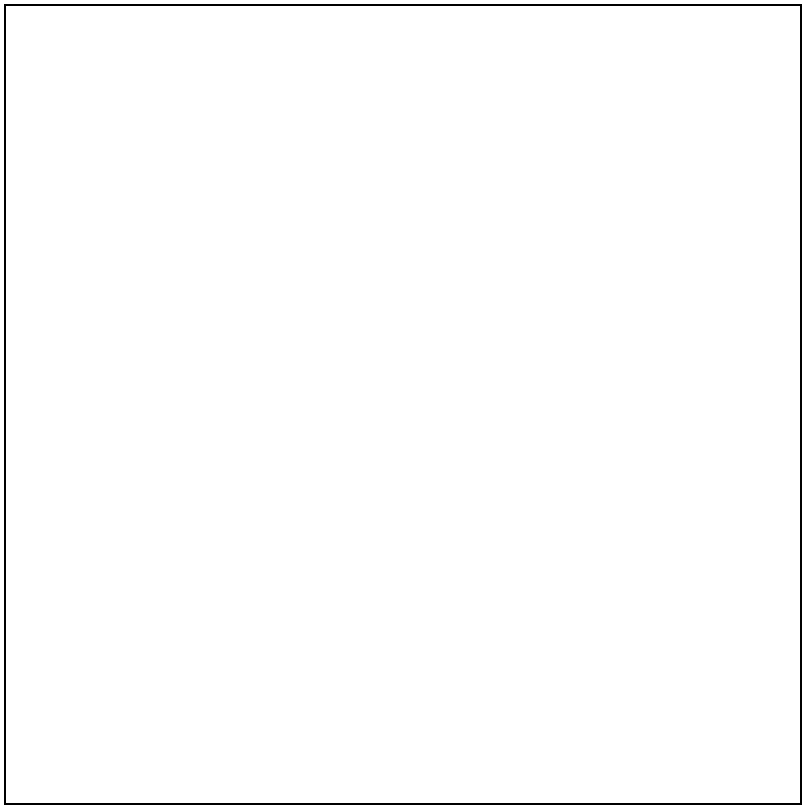

Au: Please provide fig. 14.4

Fig. 14.4 Equivalent thermodynamic cycle of Eqs. 14.10 and 14.11. The steps corresponding to Eqs. 14.11a, 14.11b, and 14.11c are illustrated separately. Adapted from Garofoli and Jordan (2003) with permission.

dielectric. A water molecule, at a specified axial distance from the channel–water interface, but otherwise free to move, mutates into an ion; simultaneously an ion in the dielectric, but far from the channel, turns into a water molecule. Standard thermodynamic perturbation determines the associated free energy, thus accounting for how differences in a peptide's interaction with water and ions leads to structural reorganization (Dorman and Jordan, 2003; Garofoli and Jordan, 2003; Dorman and Jordan, 2004)

$$\Delta G_{\text{structural}} = \int_0^1 d\lambda \left\langle \frac{dH}{d\lambda} \right\rangle, \tag{14.12a}$$

where

$$\langle(\cdots)\rangle = \frac{1}{Z} \int_{(\Omega)} d\Omega(\cdots) \exp[-\beta H(\Omega, \lambda)] \tag{14.12b}$$

is the canonical statistical average. $H(\Omega, \lambda)$ is the system Hamiltonian, Ω the complete set of phase space variables, λ the mutational variable and Z the corresponding partition function with $\beta \equiv 1/k_B T$ (k_B is Boltzmann's constant and T is absolute temperature). In the perturbation process, one channel water mutates to an ion, gradually changing its charge distribution according to the prescription

$$\lambda q_{\text{ion}} + (1 - \lambda)\rho_{\text{water}}, \tag{14.13}$$

where ρ_{water} is the charge distribution in the model water molecule, q_{ion} is the ionic charge and λ varies from 0 to 1. The Hamiltonian for channel reorganization is

$$\begin{aligned} H_{\text{channel}}(\lambda) = {} & H_{\text{V}}(\lambda) + H_{\text{W}} + H_{\text{pep}} + H_{\text{W,pep}} \\ & + H_{\text{V,W}}(\lambda) + H_{\text{V,pep}}(\lambda) + H_{\text{hard-core}}, \end{aligned} \tag{14.14}$$

where $H_{\text{V}}(\lambda)$ describes interaction of the variable species with its reaction field. H_{W}, H_{pep}, and $H_{\text{W,pep}}$ account for water–peptide interactions, $H_{\text{V,W}}(\lambda)$ and $H_{\text{V,pep}}(\lambda)$ describe interaction between the variable species, water and peptide, in all cases including reaction field influences. The hard-core term keeps species apart.

In the bubble geometry of Fig. 14.2c, the perturbation procedure is different. The parameterization procedure relies on solvating an ion in a small, but sufficiently large "aqueous sphere" containing a limited number of model water molecules (Dorman and Jordan, 2003). Instead of mutation passing through a vacuum intermediate, channel water changes to an ion and an ion in the computational sphere simultaneously turns into a water molecule; the corresponding Hamiltonian is analogous to Eq. 14.14, with peptide contributions deleted. All changes take place in an electrical background with $\varepsilon \equiv 2$. The thermodynamic exchange process is

$$\text{Ion}_{\text{sphere}} + \text{Water}_{\text{channel}} \rightarrow \text{Ion}_{\text{channel}} + \text{Water}_{\text{sphere}}. \tag{14.15}$$

There is still a Born-like contribution, since ion and water solvation cavities differ slightly in size in the "aqueous sphere" and channel environments. The total free energy change in transferring an ion from bulk water to the channel is given by Eq. 14.12a plus an elaboration of Eqs. 14.9a and 14.9b. Instead of the hydration and vaporization terms of Fig. 14.4 there are cavity terms describing the ionic and water environments in the "aqueous sphere," i.e., the changes in the size of the solvation cavities. The associated Born energy is

$$\Delta G_{\text{Born}} = \frac{e_o^2}{2\varepsilon}\left(\frac{1}{R_{\text{channel}}} - \frac{1}{R_{\text{sphere}}}\right) + \Delta G_{\text{water cavity}}(\text{channel} \rightarrow \text{sphere}), \tag{14.16}$$

where R_{sphere} and R_{channel} are cavity radii for the ion in the two regions; the second term in Eq. 14.16 accounts for the energy needed to change the size of water's

solvation cavity (Beveridge and Schnuelle, 1975). These are determined by evaluating the mean distance between the variable species and its surroundings at the start and conclusion of the complementary thermodynamic perturbations (Dorman and Jordan, 2003, 2004).

14.7 Applications

14.7.1 Deconvoluting Structural Influences

The SMC method is ideal for "*gedanken*" experiments based on reengineered channel architectures, allowing an assessment of how individual structural features influence ion permeation. While protein parameters are constrained, hypothetical scenarios can provide insight into structural evolution.

One example, focusing on the role of the water cavity in potassium channels, is illustrative. The five single file sites of Fig. 14.1 model possible ion binding locations (Morais-Cabral et al., 2001; Zhou et al., 2001), of which sites 1–3 are most important (Doyle et al., 1998). In treating potassium channel permeation energetics with the geometry of Fig. 14.1, these three positions are better modeled because explicit water molecules act as buffers separating them from the nearby Helmholtz layer. To stress the conditional nature of predictions for the outer sites, where energetics is sensitive to the nearby dielectric discontinuity, they are designated 0* and 4*. Ion(s), channel waters, and the selectivity filter carbonyls are mobile; more distant electrical sources are fixed (Garofoli and Jordan, 2003).

The spherical water pool is only a rough approximation to the inner pore of potassium channels. The KcsA crystal ~~was~~ captured ~~it~~ in a nonconductive form, its inner mouth too narrow to permit ion entry (Doyle et al., 1998). Gating opens the channel, altering its structure drastically; the small water pool must deform into a vestibule into which bulk water can diffuse freely. The crystal structure of such a channel illustrates this clearly (Jiang et al., 2002). On its intracellular side, the channel is greatly deformed, but the selectivity filter region outside the water pool remains essentially unchanged (Jiang et al., 2002). Consequently, using the structure of the "closed" state filter to analyze permeation energetics in the "open" state is not unreasonable. The SMC approach does this in two ways: (1) by reducing membrane thickness, bringing the cytoplasm ever closer to the cavity, in essence shortening the inner pore; (2) by deforming the cavity into a cylindrical tube extending to the cytoplasm and filled with 72 explicit waters. Regardless of the size of the buffer domain or the amount of water it contains, ion energetics in the carbonyl binding pockets is essentially unaltered (Garofoli and Jordan, 2003). The cavity insulates ions in the filter from changes in inner pore geometry, guaranteeing that filter operation is essentially unperturbed by structural changes in the channel's inner pore. Only at site 4*, the filter-cavity boundary, does altering inner pore structure have any effect, which is totally consistent with observed behavior in the potassium channel family. Unitary conductances, which depend on the size of the inner pore (Chung

Au: Please check the sentence "The KcsA crystal was . . . permit ion entry" for clarity.

et al., 2002b), vary by two orders of magnitude but are essentially uncorrelated with channel selectivity (Hille, 2001).

14.7.2 Selectivity in the Potassium Channel Filter

SMC modeling permits ready analysis of filter selectivity, by mutational transformation among the four larger alkali cations. The focus remains on the interior ionic sites numbered 1–3, which are most reliably modeled. Such studies provide useful insights at modest computational cost.

While there is compelling evidence that the filter is always multiply occupied in KcsA, SMC analysis permits another thought experiment: direct comparison of alkali cation energetics in the interior of the singly occupied filter, a condition that is possibly experimentally realized in the delayed rectifier channel, $K_v2.1$ (Consiglio and Korn, 2004; Immke et al., 1999). At the three interior sites sodium occupancy is unfavorable relative to potassium by $\sim$10–15kT, for $T = 300$ K, values in reasonable agreement with standard simulational analysis (Allen et al., 2000; Bernèche and Roux, 2001; Luzhkov and Åqvist, 2001). In the SMC approach the energetic influence of solvent structural reorganization is separable from that due to ion transfer between surroundings of different permittivity; the two terms are given by Eqs. 14.12 and 14.9, respectively. SMC comparison of sodium and potassium energetics indicates that the ion transfer term exerts the larger effect on the filter's ability to discriminate (Garofoli and Jordan, 2003). As seen in Table 14.1, sodium is less well cradled in its solvation cavity than potassium. This is consonant with MacKinnon's original idea (Doyle et al., 1998) and the earlier "close fit" hypothesis (Bezanilla and Armstrong, 1972), but differs from a recent simulational interpretation (Noskov et al., 2004) that is conceptually similar to Eisenman's early interpretation of selectivity (Eisenman, 1962).

SMC analysis of a multiply occupied filter yields no surprises (Garofoli and Jordan, 2003). Consonant with experiment (Hille, 2001) rubidium occupancy is roughly as likely as that of potassium, but cesium is significantly less stable in the filter, mainly reflecting a relatively unfavorable reorganizational free energy. Ionic energetics at site 4*, the filter-cavity boundary, is illuminating. Here the filter no longer imposes a severe structural constraint and the scaffolding can deform more

Table 14.1 Mean ionic cavity radii (in Å) for various cations at the KcsA filter sites of Fig. 14.1.

	Site 1	Site 2	Site 3	Site 4*
Na^+	1.23	1.24	1.23	1.03
K^+	1.38	1.43	1.40	1.32
Rb^+	1.57	1.48	1.50	1.44
Cs^+	1.65	1.61	1.66	1.56
Ba^{2+}	1.43	1.44	1.43	1.38

readily. Both sodium and possibly barium can compete effectively with potassium, consistent with experiment (Bezanilla and Armstrong, 1972; French and Wells, 1977; Yellen, 1984; Neyton and Miller, 1988a,b; Heginbotham et al., 1999; Jiang and MacKinnon, 2000).

14.7.3 Gramicidin Permeability

The inability of standard simulational methods to account for permeation energetics in gramicidin A has been perplexing to theorists. As discussed in the introduction, PMF determinations with conventional force fields yield free energy barriers of $\sim 20kT(T = 300\,\mathrm{K})$, implying conductances $\sim 10^7$ times too small. Since gramicidin is structurally far better characterized than any other channel (Arseniev et al., 1985; Ketchem et al., 1997), this discrepancy is dismaying. SMC analysis provides an alternative perspective to more familiar methods. Unlike the case of conventional MD simulations, electronic polarization is taken into account and the reaction field problem can be solved without approximation.

Gramicidin's permeation pathway is a water-filled pore bounded by a cylindrical scaffolding formed by the peptide's hydrogen bonded backbone, with its amino acid residues embedded in the surrounding lipid (Arseniev et al., 1985; Ketchem et al., 1997). SMC studies using the electrical geometry of Fig. 14.2c, treat the ion, channel waters, and carbonyls and amides of the backbone as mobile; the peptide's aryl residues and the membrane dipoles (Thompson et al., 2001) impose a fixed background potential. A correction is used to compensate for Fig. 14.2c's semi-infinite geometry. SMC calculations of permeation free energies for the larger alkali cations and chloride yield results, which, while imperfect, are in fair agreement with experiment. Cation binding occurs at the proper location, ∼1.0 nm from the channel midpoint. The correct selectivity sequence is observed with rubidium the most permeable cation and chloride passage forbidden. Instead of cation conductances seven orders of magnitude low, discrepancies are greatly reduced, to no more than ∼100, as shown in Table 14.2 (Dorman and Jordan, 2004).

Table 14.2 Ionic conductances (pS) of gramicidin A in 0.1 M electrolyte, based on total permeation free energy profiles determined using GROMOS and CHARMM19 partial charge parameters. Conductances were computed using Levitt's (Levitt, 1986) single-file algorithm. Simulational values are estimated from the free energy profiles of Edwards et al. (2002).

	GROMOS	CHARMM19	Experiment[a]
K^+	0.24	0.025	11
Rb^+	12.	0.40	20
Cs^+	1.0	0.074	18
Cl^-	2.4×10^{-8}	6.0×10^{-6}	0
Simulation, K^+	1.8×10^{-7}	4.2×10^{-7}	11

[a] Data extrapolated from Fig. 5 of Andersen (1983).

Au: What do you mean by 12.

The electrical decomposition procedure illustrates how the aryl residues and membrane dipoles influence cation conductance. Ionic interaction with the aryl residues creates the binding site. The membrane dipoles substantially reduce cation conductance. A thought experiment based on variation of the SMC parameters helps explain why standard simulational approaches are plagued with difficulties. Reducing ε_I to 1 eliminates the mean contribution of electronic polarization; this increases the internal permeation free energy barrier by $\sim 8kT$, nearly half the error in computations based on standard force fields (Allen et al., 2003).

14.8 Final Observations

SMC modeling is a blunt tool. It is an alternative to standard simulational procedures, affording complementary insights. It accommodates electronic polarization in a mean field sense and, by introducing specially designed dielectric geometries, treats long-range electrostatics exactly. However, it must be used cautiously, as electronic environments in nonuniform surroundings like peptide–lipid–water ensembles are far from uniform. To further exploit this idea requires development of a better SMC force field. The procedure used here is too simple. The peptide force field is rudimentary and the water model is primitive. As a result only the larger cations and halides have been reliably parameterized and conclusions must be viewed as qualitative. Extensions lifting these limitations so that peptides are more accurately described and so that sodium and the alkaline earth cations could be more reliably modeled would be valuable.

Acknowledgments

I thank Michael Partensky and Gennady Miloshevsky for helpful commentary. This work was supported by a grant from the National Institutes of Health, GM-28643.

References

Aksimentiev, A., and K. Schulten. 2005. Imaging {alpha}-hemolysin with molecular dynamics: Ionic conductance, osmotic permeability, and the electrostatic potential map. *Biophys. J.* 88:3745–3761.

Allen, T.W., O.S. Andersen, and B. Roux. 2004. Energetics of ion conduction through the gramicidin channel. *Proc. Natl. Acad. Sci. USA* 101:117–122.

Allen, T.W., T. Bastug, S. Kuyucak, and S.H. Chung. 2003. Gramicidin a channel as a test ground for molecular dynamics force fields. *Biophys. J.* 84:2159–2168.

Allen, T.W., A. Bilznyuk, A.P. Rendell, S. Kuyucak, and S.H. Chung. 2000. The potassium channel: Structure, selectivity and diffusion. *J. Chem. Phys.* 112:8191–8204.

Andersen, O.S. 1983. Ion movement through gramicidin A channels. Single-channel measurements at very high potentials. *Biophys. J*. 41:119–133.

Arseniev, A.S., I.L. Barsukov, V.F. Bystrov, A.L. Lomize, and Y.A. Ovchinnikov. 1985. 1H-NMR study of gramicidin A transmembrane ion channel. Head-to-head right-handed, single-stranded helices. *FEBS Lett*. 186:168–174.

Beglov, D., and B. Roux. 1994. Finite representation of an infinite bulk system—solvent boundary potential for computer-simulations. *J. Chem. Phys*. 100:9050–9063.

Berendsen, H.J.C., J.P.M. Postma, W.F. van Gunsteren, and J. Hermans. 1981. Interaction models for water in relation to protein hydration. *In*: Intermolecular Forces. B. Pullman editor. Reidel, Dordrecht, pp. 331–342.

Bernèche, S., and B. Roux. 2001. Energetics of ion conduction through the K^+ channel. *Nature* 414:73–77.

Bernèche, S., and B. Roux. 2003. A microscopic view of ion conduction through the K^+ channel. *PNAS* 100:8644–8648.

Beveridge, D.L., and G.W. Schnuelle. 1975. Free energy of a charge distribution in concentric dielectric continua. *J. Phys. Chem.* 79:2562–2566.

Bezanilla, F., and C.M. Armstrong. 1972. Negative conductance caused by entry of sodium and cesium ions into the potassium channels of squid axon. *J. Gen. Physiol*. 60:588–608.

Born, M. 1920. Volumen und hydrationswarme der Ionen. *Zeit. für Physik*. 1:45–48.

Burykin, A., C.N. Schutz, J. Villa, and A. Warshel. 2002. Simulations of ion current in realistic models of ion channels: The KcsA potassium channel. *Proteins* 47:265–280.

Chen, D.P., V. Barcilon, and R.S. Eisenberg. 1992. Constant fields and constant gradients in open ionic channels. *Biophys. J*. 61:1372–1393.

Chung, S.H., T.W. Allen, M. Hoyles, and S. Kuyucak. 1999. Permeation of ions across the potassium channel: Brownian dynamics studies. *Biophys. J*. 77:2517–2533.

Chung, S.H., T.W. Allen, and S. Kuyucak. 2002a. Conducting-state properties of the KcsA potassium channel from molecular and Brownian dynamics simulations. *Biophys. J*. 82:628–645.

Chung, S.H., T.W. Allen, and S. Kuyucak. 2002b. Modeling diverse range of potassium channels with Brownian dynamics. *Biophys. J*. 83:263–277.

Consiglio, J.F., and S.J. Korn. 2004. Influence of permeant ions on voltage sensor function in the Kv2.1 potassium channel. *J. Gen. Physiol*. 123:387–400.

Cornell, W.D., P. Cieplak, C.I. Bayly, I.R. Gould, K.M. Merz, D.M. Ferguson, D.C. Spellmeyer, T. Fox, J.W. Caldwell, and P.A. Kollman. 1995. A 2nd generation force-field for the simulation of proteins, nucleic-acids, and organic-molecules. *J. Am. Chem. Soc*. 117:5179–5197.

Corry, B., S. Kuyucak, and S.H. Chung. 2000. Tests of continuum theories as models of ion channels. II. Poisson–Nernst–Planck theory versus Brownian dynamics. *Biophys. J*. 78:2364–2381.

Corry, B., M. O'Mara, and S.-H. Chung. 2004. Conduction mechanisms of chloride ions in ClC-type channels. *Biophys. J.* 86:846–860.

Dorman, V., M.B. Partenskii, and P.C. Jordan. 1996. A semi-microscopic Monte Carlo study of permeation energetics in a gramicidin-like channel: The origin of cation selectivity. *Biophys. J.* 70:121–134.

Dorman, V.L., and P.C. Jordan. 2003. Ion–water interaction potentials in the semi-microscopic model. *J. Chem. Phys*. 118:1333–1340.

Dorman, V.L., and P.C. Jordan. 2004. Ionic permeation free energy in gramicidin: A semimicroscopic perspective. *Biophys. J.* 86:3529–3541.

Doyle, D.A., J. Morais-Cabral, R.A. Pfuetzner, A. Kuo, J.M. Gulbis, S.L. Cohen, B.T. Chait, and R. MacKinnon. 1998. The structure of the potassium channel: Molecular basis of K^+ conduction and selectivity. *Science* 280:69–77.

Edwards, S., B. Corry, S. Kuyucak, and S.H. Chung. 2002. Continuum electrostatics fails to describe ion permeation in the gramicidin channel. *Biophys. J*. 83:1348–1360.

Eisenberg, R.S. 1999. From structure to function in open ionic channels. *J. Membr. Biol.* 171:1–24.

Eisenman, G. 1962. Cation selective glass electrodes and their mode of operation. *Biophys. J*. 2(2, Pt 2):259–323.

Fettiplace, R., D.M. Andrews, and D.A. Haydon. 1971. Thickness, composition and structure of some lipid bilayers and natural membranes. *J. Membr. Biol*. 5:277–296.

French, R.J., and J.B. Wells. 1977. Sodium ions as blocking agents and charge carriers in the potassium channel of squid giant axon. *J. Gen. Physiol*. 70:707–724.

Garofoli, S., and P.C. Jordan. 2003. Modeling permeation energetics in the KcsA potassium channel. *Biophys. J*. 84:2814–2830.

Grunwald, E. 1996. Thermodynamics of Molecular Species. Wiley-Interscience, New York.

Hasted, J.B. 1973. In F. Franks, editor. Water, a Comprehensive Treatise, Vol. 1. Plenum, New York, pp. 405–458.

Heginbotham, L., M. LeMasurier, L. Kolmakova-Partensky, and C. Miller. 1999. Single ~~streptomyces lividans~~ K(+) channels: Functional asymmetries and sidedness of proton activation. *J. Gen. Physiol*. 114:551–560.

Hille, B. 2001. Ionic Channels of Excitable Membranes, 3rd Ed. Sinauer Associates, Sunderland, MA.

Im, W., and B. Roux. 2002. Ion permeation and selectivity of OmpF porin: A theoretical study based on molecular dynamics, Brownian dynamics, and continuum electrodiffusion theory. *J. Mol. Biol.* 322:851–869.

Immke, D., M. Wood, L. Kiss, and S.J. Korn. 1999. Potassium-dependent changes in the conformation of the Kv2.1 potassium channel pore. *J. Gen. Physiol*. 113:819–836.

Jackson, J.D. 1962. Classical Electrodynamics. John Wiley, New York.

Jiang, Y., A. Lee, J. Chen, M. Cadene, B.T. Chait, and R. MacKinnon. 2002. The open pore conformation of potassium channels. *Nature* 417:523–526.

Jiang, Y., and R. MacKinnon. 2000. The barium site in a potassium channel by ~~x~~-ray crystallography. *J. Gen. Physiol.* 115:269–272.

Au: Please provide the chapter title of the book.

Jordan, P.C. 2005. Semimicroscopic modeling of permeation energetics in ion channels. *IEEE Trans. Nanobiosci*. 4:94–101.

Jordan, P.C., M.B. Partenskii, and V. Dorman. 1997. Electrostatic influences on ion–water correlation in ion channels. *Prog. Cell Res*. 6:279–293.

Ketchem, R., B. Roux, and T. Cross. 1997. High-resolution polypeptide structure in a lamellar phase lipid environment from solid state NMR derived orientational constraints. *Structure* 5:1655–1669.

King, G., and A. Warshel. 1989. A surface constrained all-atom solvent model for effective simulations of polar solutions. *J. Chem. Phys*. 91:3647–3661.

Kornyshev, A.A. 1988. Solvation of a metal surface. *In*: The Chemical Physics of Solvation. R.R. Dogonadze, E. Kálmán, A.A. Kornyshev, and J. Ulstrup, editors. Elsevier, Amsterdam, pp. 355–400.

Levitt, D.G. 1986. Interpretation of biological ion channel flux data—Reaction-rate versus continuum theory. *Annu. Rev. Biophys. Biophys. Chem*. 15:29–57.

Luzhkov, V.B., and J. Åqvist. 2001. K(+)/Na(+) selectivity of the KcsA potassium channel from microscopic free energy perturbation calculations. *Biochim. Biophys. Acta* 1548:194–202.

MacKerell, A.D., D. Bashford, M. Bellott, R.L. Dunbrack, J.D. Evanseck, M.J. Field, S. Fischer, J. Gao, H. Guo, S. Ha, D. Joseph-McCarthy, L. Kuchnir, K. Kuczera, F.T.K. Lau, C. Mattos, S. Michnick, T. Ngo, D.T. Nguyen, B. Prodhom, W. E. Reiher, B. Roux, M. Schlenkrich, J.C. Smith, R. Stote, J. Straub, M. Watanabe, J. Wiorkiewicz-Kuczera, D. Yin, and M. Karplus. 1998. All-atom empirical potential for molecular modeling and dynamics studies of proteins. *J. Phys. Chem. B* 102:3586–3616.

Miloshevsky, G.V., and P.C. Jordan. 2004. Anion pathway and potential energy profiles along curvilinear bacterial ClC Cl^- pores: Electrostatic effects of charged residues. *Biophys. J*. 86:825–835.

Morais-Cabral, J.H., Y. Zhou, and R. MacKinnon. 2001. Energetic optimization of ion conduction rate by the K^+ selectivity filter. *Nature* 414:37–42.

Moy, G., B. Corry, S. Kuyucak, and S.H. Chung. 2000. Tests of continuum theories as models of ion channels. I. Poisson–Boltzmann theory versus Brownian dynamics. *Biophys. J*. 78:2349–2363.

Neyton, J., and C. Miller. 1988a. Discrete Ba^{2+} block as a probe of ion occupancy and pore structure in the high-conductance Ca^{2+} -activated K^+ channel. *J. Gen. Physiol*. 92:569–586.

Neyton, J., and C. Miller. 1988b. Potassium blocks barium permeation through a calcium-activated potassium channel. *J. Gen. Physiol*. 92:549–567.

Noskov, S.Y., S. Berneche, and B. Roux. 2004. Control of ion selectivity in potassium channels by electrostatic and dynamic properties of carbonyl ligands. *Nature* 431:830–834.

Papazyan, A., and A. Warshel. 1998. Effect of solvent discreteness on solvation. *J. Phys. Chem. B* 102:5348–5357.

Partenskii, M.B., and P.C. Jordan. 1992. Theoretical perspectives on ion-channel electrostatics: Continuum and microscopic approaches. *Q. Rev. Biophys*. 25:477–510.

Pauling, L. 1960. The Nature of the Chemical Bond, 3rd Ed. Cornell University Press, Ithaca, NY.

Thompson, N., G. Thompson, C.D. Cole, M. Cotten, T.A. Cross, and D.D. Busath. 2001. Noncontact dipole effects on channel permeation. IV. Kinetic model of 5F-~~Trp(13)~~ gramicidin A currents. *Biophys. J*. 81:1245–1254.

van Gunsteren, W.F., and H.J.C. Berendsen. 1987. Groningen Molecular Simulations (GROMOS) Library Manual. Biomos, Groningen, NL.

Warshel, A. 1979. Calculations of chemical processes in solutions. *J. Phys. Chem*. 83:1640–1652.

Yellen, G. 1984. Relief of Na^+ block of Ca^{2+}-activated K^+ channels by external cations. *J. Gen. Physiol*. 84:187–199.

Zhou, Y., J. H. Morais-Cabral, A. Kaufman, and R. MacKinnon. 2001. Chemistry of ion coordination and hydration revealed by a K^+ channel-Fab complex at 2.0 ~~A~~ resolution. *Nature* 414:43–48.